The multifractal spectrum for the solar wind flow

Wiesław M. Macek

Faculty of Mathematics and Science, Cardinal Stefan Wyszyński University in Warsaw, Dewajtis 5, 01-815 Warszawa; Space Research Centre, Polish Academy of Sciences, Bartycka 18 A, 00-716 Warszawa, Poland

Abstract. We analyze time series of velocities of the low-speed stream of the solar wind plasma including Alfvénic fluctuations measured in situ by the Helios spacecraft in the inner heliosphere. We demonstrate that the influence of noise in the data can be efficiently reduced by a moving average filter. We calculate the multifractal spectrum for the solar wind flow directly from the cleaned experimental signal. We also show that due to nonlinear noise reduction we get with much reliability estimates of the Kolmogorov entropy and the largest Lyapunov exponent. For intermediate length scales the Lyapunov exponent and the entropy are plausibly positive locally, which exhibits sensitivity to initial conditions. This shows that the slow solar wind in the inner heliosphere is most likely a deterministic chaotic system, where noise is not dominant.

The generalized dimensions of attractors are important characteristics of *complex* dynamical systems [1]. Since these dimensions are related to frequencies with which typical orbits in phase space visit different regions of the attractors, they provide information about dynamics of the systems [2]. If the measure has different fractal dimensions on different parts of the support, the measure is multifractal [3].

Following space physics applications, e.g., [4, 5], we consider the inner heliosphere. The solar wind plasma flowing supersonically outward from the Sun is quite well modeled within the framework of the hydromagnetic theory. This continuous flow has two forms: slow (≈ 300 km s^{-1}) and fast (≈ 900 km s^{-1}) [6]. The fast wind is associated with coronal holes and is relatively uniform and stable, while the slow wind is quite variable in terms of velocities. We limit our study to the low-speed stream. Indication for a chaotic attractor in the slow solar wind has been given in [7, 8, 9, 10]. In particular, Macek [7] has calculated the correlation dimension of the reconstructed attractor and has provided tests for *nonlinearity* in the solar wind data, including a powerful method of statistical surrogate data tests [11]. Further, Macek and Redaelli [9] have shown that the Kolmogorov entropy of the attractor is *positive* and finite, as it holds for a *chaotic* system. The entropy is plausibly constrained by a *positive* local Lyapunov exponent that would exhibit sensitive dependence on initial conditions of the system.

Recently, we have extended our previous results on the dimensional time series analysis [7]. Namely, we have applied the technique that allows a realistic calculation of the generalized dimensions of the solar wind flow, directly from the cleaned experimental signal by using the Grassberger and Procaccia method [12]. The resulting spectrum of dimensions shows multifractal structure of the solar wind in the inner heliosphere [10]. The obtained multifractal spectrum is consistent with that for the multifractal measure on the self-similar weighted Cantor set. In this paper we demonstrate the influence of noise on these results and show that noise can efficiently be reduced by a simple moving average filter.

We analyze the Helios data using plasma parameters measured *in situ* in the heliosphere near the Sun, at 0.3 AU, Ref. [6]. The radial velocity component of the plasma flow, v, has been investigated in [7, 9]. In this paper we also analyze one of the so-called Elssäser variables $x = v + v_A$, where $v_A = B/(\mu_o \rho)^{1/2}$ is the Alfvénic velocity calculated from the experimental data: the radial component of the magnetic field of the plasma B and the mass density ρ (μ_o is the permeability of free space). These raw data of $N = 4,513$ points, with sampling time of $\Delta t = 40.5$ s, are shown in Figure 1 (a).

As in [10], slow trends ($420.06 - 15.4\ t - 82.31\ t^2$, with t being a fraction of total sample) were subtracted from the original data $x_i = v(t_i) + v_A(t_i)$, in km s^{-1}, $i = 1, \ldots, N$ and the data with the initial several percent noise level, were (8-fold) smoothed (replacing each data point with the average of itself and its two nearest neighbors). The detrended and smoothed data are shown in Figure 1 (b) of Ref. [10]. Certainly, this moving average filter removes considerable amount of noise, leaving only about 1%. The nonlinear filtering, which allows calculation of the entropy, has been discussed in [9]. It has been shown that after the nonlinear Schreiber filter the calculated dimension has been somewhat reduced. In this paper, we focus on the calculations of dimensions.

CP679, *Solar Wind Ten: Proceedings of the Tenth International Solar Wind Conference,*
edited by M. Velli, R. Bruno, and F. Malara

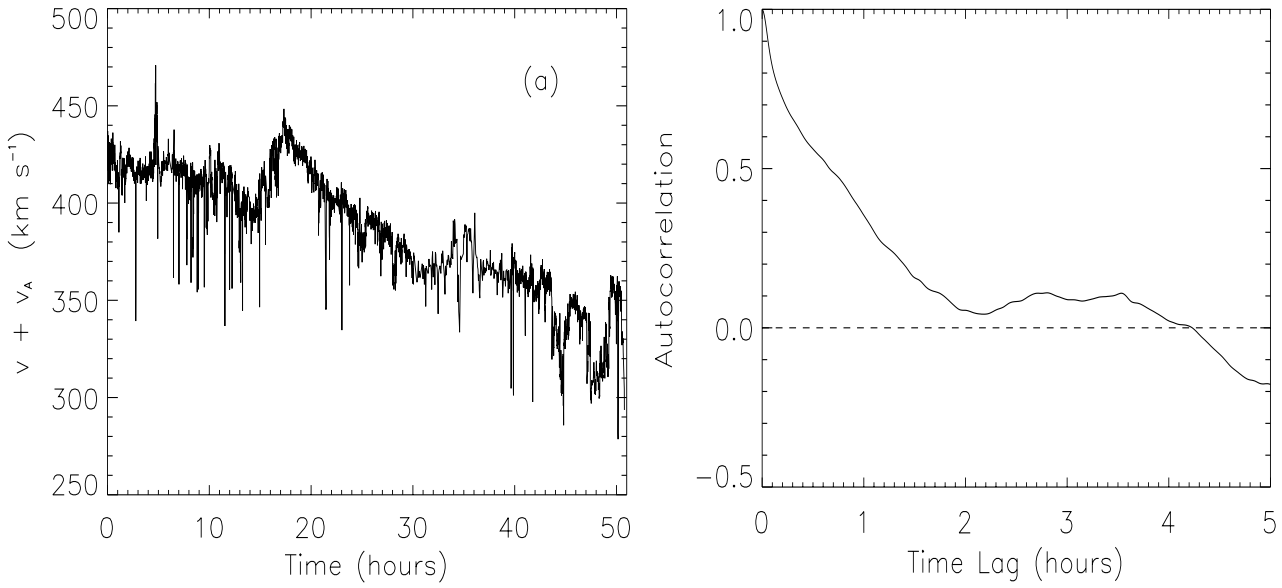

FIGURE 1. (a) The flow velocity with included Alfvénic velocity, $v + v_A$ (Elssäser variable) observed by the Helios 1 spacecraft in 1975 from 67:08:20.5 to 69:11:07 (day:h:min) at distances 0.32 AU from the Sun, for the raw data, (b) the normalized autocorrelation function as a function of the time lag for the detrended and smoothed data.

Therefore, we use moving average filtering, cf. [7].

Table 1, taken from Ref. [10], summarizes selected calculated characteristics of the detrended data cleaned by using the moving average filter. The probability distributions are clearly non-Gaussian. We have a large skewness of ~ 0.26 (as compared with its normal standard deviation 0.06) and a very large kurtosis of 0.88 (the latter was small for the analysis with no magnetic field), cf. Ref [7]. We have also estimated Lempel-Ziv measure of *complexity*, relative to white noise [13]. The calculated value ~ 0.17 is even smaller than in [7] (≈ 0.20); maximal complexity, or randomness, would have a value of 1.0, while a value of zero denotes perfect deterministic nonlinear predictability.

As shown in Figure 1 (b), the normalized autocorrelation function first fells steeply by a factor of $1/\mathrm{e}$ in one-third of hour then decreases nearly linearly (reaching a value of $1/2$ at $2/3$ h) to $1/\mathrm{e}$ at $t_a \approx 1$ h, cf. [8, a lower inset to Fig. 1] (see also Table 1). Obviously, for a periodic system the optimum time delay for attractor reconstruction would be one-quarter of the natural orbital period, i. e., the first zero of the autocorrelation function. Therefore, we choose a time delay $\tau = 150\,\Delta t$, where the autocorrelation function has the first minimum and its value is very small. This value is smaller than $t_0 = 376\,\Delta t$, the first zero of the autocorrelation function, $(\langle x(t)x(t+t_0)\rangle - \langle x(t)\rangle^2)/\sigma^2 = 0$ with average velocity $\langle x\rangle = -0.36$ km s^{-1} and standard deviation $\sigma = 8.54$ km s^{-1}, cf. also t_a in Table 1 when the autocorrelation function decreases to $1/\mathrm{e}$.

Using our time series of equally spaced, detrended and cleaned data, we construct a large number of vectors $\mathbf{X}(t_i) = [x(t_i), x(t_i+\tau), \ldots, x(t_i+(m-1)\tau)]$ in the embedding phase space of dimension m, where $i = 1, \ldots, n$ with $n = N - (m-1)\tau$. Then, we divide this space into a large number $M(r)$ of equal hypercubes of size r which cover the presumed attractor. If p_j is the probability measure that a point from a time series falls in a typical j-th hypercube, using the q-order function $I_q(r) = \sum (p_j)^q$, $j = 1, \ldots, M$, the q-order generalized dimension is given by [2]

$$D_q = \frac{1}{q-1} \lim_{r\to 0} \frac{\ln I_q(r)}{\ln r}\,, \qquad (1)$$

We see from Eq. (1) that the larger q is, the more strongly are the higher probability cubes (visited more frequently by a trajectory) weighted in the sum for $I_q(r)$. Only if $q = 0$, all the cubes are counted equally, $I_o = M$, and we recover the box-counting dimension, D_0.

Writing $I_q(r) = \sum p_j (p_j)^{q-1}$ as a weighted average $\langle (p_j)^{q-1}\rangle$, one can associate bulk with the generalized average probability per hypercube $\mu = \sqrt[q-1]{\langle (p_j)^{q-1}\rangle}$, and identify D_q as a scaling of bulk with size, $\mu \propto r^{D_q}$. Since the data cannot constrain well the capacity dimension D_0, we look for higher order dimensions, which quantify the multifractality of the probability measure on the attractor. For example, the limit $q \to 1$ leads to a geometrical average (the information dimension). For $q = 2$ the generalized average is the ordinary arithmetic average (the standard correlation dimension), and for $q = 3$ it

TABLE 1. Characteristics of the solar wind, $v + v_A$, filtered data.

	Smoothed	Shuffled data	Shuffled phases
Skewness, κ_3	0.26	0.26	-0.26
Kurtosis, κ_4	0.88	0.88	0.26
Relative complexity	0.17	1.0	0.23
Autocorrelation time, t_a	3.5×10^3 s	40 s	3.3×10^3 s
Capacity dimension, D_0	4.4	5.8	4.6
Information dimension, D_1	4.0	5.0	4.5
Correlation dimension, D_2^*	3.5	5.2	4.6

* The average slope for $6 \leq m \leq 8$ is taken as D_2.

is a root-mean-square average. In practice, for a given m and r,

$$p_j \simeq \frac{1}{n-2n_c-1} \sum_{i=n_c+1}^{n} \theta(r - \mid \mathbf{X}(t_i) - \mathbf{X}(t_j) \mid) \quad (2)$$

with $\theta(x)$ being the unit step function, and $n_c = 2$ is the Theiler's correction [14]. Finally, $I_q(r)$ is taken to be equal to the generalized q-point correlation sum [12]

$$C_q(m,r) = \frac{1}{n_{\rm ref}} \sum_{j=1}^{n_{\rm ref}} (p_j)^{q-1}, \quad (3)$$

where $n_{\rm ref} = 500$ is the number of reference vectors. For large dimensions m and small distances r in the scaling region it can be argued that $C_q(m,r) \propto r^{(q-1)D_q}$, where D_q is an approximation of the ideal limit $r \to 0$ in Eq. (1) for a given q, Ref. [12].

First, we calculate the natural logarithm of the standard ($q = 2$) correlation sum $C_m(r) = C_2(m,r)$ versus $\ln r$ (normalized) for various embedding dimensions: $m =$ 4 (dotted curve), $m = 5$ (diamonds), 6 (triangles), 7 (squares), and 8 (crosses) signs. The slopes $D_{2,m}(r) = {\rm d}[\ln C_m(r)]/{\rm d}(\ln r)$ in the scaling region of r should provide the correlated dimension. The results obtained using the moving average filter are presented in Figure 2, while those obtained using the singular-value decomposition and nonlinear Schreiber filters have been discussed in [7, 9]. Since the correlation sum is simply an arithmetic average over the numbers of neighbors, this can yield meaningful results for the dimension even when the number of neighbors available for some reference points is limited in most real dynamical systems. If the D-dimensional attractor exists, we expect a plateau of the slopes for $m \geq D$ and in the worst case for $m > 2D$. For m large enough an average slope in the scaling region indicates a proper correlation dimension D_2. We have a clear plateau which appears already for $m = 4$ (dotted curve) and $m = 5$. For higher dimensions, $m \geq 8$, the plateau is still present but more smeared out by the statistical fluctuations at small r. In our case the slope of the calculated correlation sum saturates for $m > 5$, with an average for $6 \leq m \leq 8$ of $D_2 = 3.5 \pm 0.1$, cf. Ref. [7]; this is consistent with the attractor of the low-dimension.

Second, the generalized dimensions D_q in Eq. (1) as a function of q are shown in Figure 3. The spectrum of dimensions shows multifractal structure of the solar wind in the inner heliosphere. For comparison, an extremely simple example of the multifractal system is the weighted Cantor set, where the probability of visiting one segment is p (say $p \leq 1/2$) and the probability of visiting the other segment is $1 - p$. In this case the results can be obtained analytically; for any q in Eq. (1) one has

$$(1-q)D_q = \log_3[p^q + (1-p)^q]. \quad (4)$$

The difference of the maximum and minimum dimension, associated with the least dense and most dense points on the attractor, correspondingly, is $D_{-\infty} - D_{\infty} = \log_3(1/p - 1)$ and in the limit $p \to 0$ this difference rises to infinity. Hence, the parameter p can be regarded as a degree of multifractality. The results of $D_q + 3$ calculated for $p = 0.1$ in Eq. (4) are also shown in Figure 3 by a dash-dotted line. We see that for $q > 1$ the multifractal spectrum of the solar wind is roughly consistent with that for the multifractal measure on the self-similar weighted Cantor set, with a single weighting parameter p. The obtained value of this parameter demonstrates that some cubes that cover the attractor of this dynamical system are visited one order of magnitudes more frequently than some other cubes, as is illustrated in our previous paper, see Figure 5 of Ref. [7].

We also estimate the Kolmogorov correlation entropy, K_2, and the largest positive Lyapunov exponent, $\lambda_{\rm max}$. The vertical spacings between the parallel lines in Figure 2 of Ref. [10] averaged in the saturation region $8 \leq m \leq 10$ are taken as K_2 yielding the value of ≈ 0.1 (per delay time τ). Using the algorithm of Ref. [15] and nonlinear noise reduction, one obtains the magnitude of $\lambda_{\rm max} \sim 0.1$ in the same units as for K_2 (base e). In general, the entropy K_q is at most the sum of the positive Lyapunov exponents $\sum \lambda_i$, e.g., [2]. The value of the Lyapunov exponent is consistent with the Kolmogorov ($q = 2$) entropy, which should be its lower

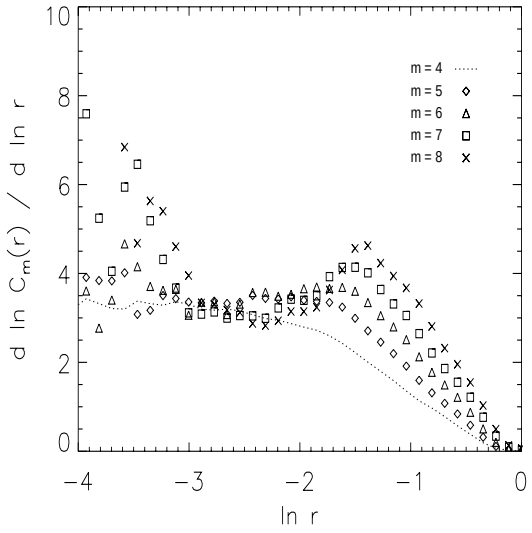

FIGURE 2. The slopes $D_{2,m}(r) = \mathrm{d}(\ln C_m(r))/\mathrm{d}(\ln r)$ for the correlation sum $C_m(r)$ versus $\ln r$ (normalized) obtained for the cleaned experimental signal for various embedding dimensions: $m = 4$ (dotted curve), $m = 5$ (diamonds), 6 (triangles), 7 (squares), and 8 (crosses).

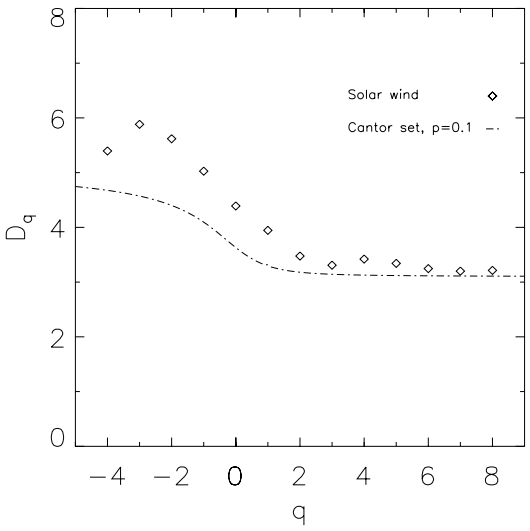

FIGURE 3. The generalized dimensions D_q in Eq. (1) as a function of q. The correlation dimension is $D_2 = 3.5 \pm 0.1$, see Table 1. The values of $D_q + 3$ calculated analytically for the weighted Cantor set with $p = 0.1$ (dash-dotted).

bound: $K_2 \leq \sum \lambda_i$ (positive). The time over which the meaningful prediction of the behavior of the system is possible is roughly $\sim 1/\lambda_{\max}$, e.g., [2]. Hence the predictability of the system is limited to hours.

The obtained measures of the attractor have been subjected to the surrogate data test [11]. As has been demonstrated in Figure 8 of Ref. [7], if the original data are indeed deterministic, analysis of these surrogate data will provide values that are statistically distinct from those derived for the original data, see also Table 1. In particular, the slope of the correlation sum increases with m (no saturation), and Lempel-Ziv complexity calculated for shuffled-data becomes clearly 1.0, as it should be for a purely stochastic system. Again, we have found that the solar wind data are sensitive to this test.

In conclusion, we have shown that the moving average filter removes some amount of noise, which is sufficient to calculate the generalized dimensions of the solar wind attractor. The obtained multifractal spectrum is consistent with that for the multifractal measure on the self-similar weighted Cantor set with a degree of multifractality of $p \sim 0.1$. The obtained characteristics of the attractor are significantly different from those of the surrogate data. Thus these results show multifractal structure of the solar wind in the inner heliosphere. Hence we suggest that there exists an inertial manifold for the solar wind, in which the system has *multifractal* structure, and where noise is certainly not dominant.

This work has been done in the framework of the European Commission Research Training Network Grant No. HPRN-CT-2001-00314.

REFERENCES

1. Hentschel, H. G. E., and Procaccia, I., Physica D, **8**, 435–444 (1983); Grassberger, P., Phys. Lett. A, **97**, 227–230 (1983); Halsey, T. C., Jensen, M. H., Kadanoff, L. P., Procaccia, I., and Shraiman, B. I., Phys. Rev. A, **33**, 1141–1151 (1986).
2. Ott, E., *Chaos in Dynamical Systems*, Cambridge University Press, Cambridge, 1993.
3. Mandelbrot, B. B., Multifractal measures, especially for the geophysicist, in *Pure and Applied Geophysics*, **131**, 5–42, Birkhäuser Verlag, Basel (1989).
4. Kurths, J., and Herzel, H., Physica D, **25**, 165–172 (1987).
5. Burlaga, L. F., Geophys. Res. Lett., **18**, 69–72 (1991).
6. Schwenn, R., Large-scale structure of the interplanetary medium, in *Physics of the Inner Heliosphere*, edited by R. Schwenn and E. Marsch, Springer-Verlag, Berlin, 1990, Vol. 20, pp. 99–182.
7. Macek, W. M., Physica D, **122**, 254–264 (1998).
8. Macek W. M., and Obojska, L., Chaos, Solitons & Fractals, **8**, 1601–1607 (1997); **9**, 221–229 (1998).
9. Macek W. M., and Redaelli, S., Phys. Rev. E, **62**, 6496–6501 (2000).
10. Macek, W. M., Multifractality and chaos in the solar wind, in *Experimental Chaos*, edited by S. Boccaletti, B. J. Gluckman, J. Kurths, L. M. Pecora, and M. L. Spano, American Institute of Physics, New York, 2002, Vol. 622, pp. 74–79.
11. Theiler, J., Eubank, S., Longtin, A., Galdrikian, B., and Farmer, J. D., Physica D, **58**, 77–94 (1992).
12. Grassberger P., and Procaccia, I. , Physica D, **9**, 189–208 (1983).
13. Kaspar, F., and Schuster, H. G., Phys. Rev. A, **36**, 842–848 (1987).
14. Theiler, J., Phys. Rev. A, **34**, 2427–2432 (1986).
15. Kantz, H., Phys. Lett. A, **185**, 77–87 (1994).